Journal Name



ARTICLE TYPE

Cite this: DOI: 10.1039/xxxxxxxxxx

Effect of Rhenium Dopants on Photocarrier Dynamics and Optical Properties of Monolayer, Few-Layer, and Bulk MoS₂

Yuanyuan Li, a,b Qingfeng Liu,b Qiannan Cui,b Zeming Qi, a Judy Z. Wu,b and Hui Zhao, b

Received Date Accepted Date

DOI: 10.1039/xxxxxxxxxx

www.rsc.org/journalname

We report a comprehensive study on the effects of rhenium doping on optical properties and photocarrier dynamics of MoS_2 monolayer and bulk samples. Monolayer and few-layer samples of Re-doped (0.6 %) and undoped MoS_2 were fabricated by mechanical exfoliation, and was studied by Raman spectroscopy, optical absorption, photoluminescence, and time-resolved differential reflection measurements. Similar Raman, absorption, and photoluminescence spectra were obtained from doped and undoped samples, indicating the Re doping at this level do not significantly alter the lattice and electronic structures. Red-shift and broadening of the two phonon Raman modes were observed, showing the lattice strain and carrier doping induced by Re. The photoluminescence yield of the doped monolayer is about 15 times lower than the undoped sample, while the photocarrier lifetime is about 20 times shorter in the doped monolayer. Both observations can be attributed to diffusion-limited Auger nonradiative recombination of photocarriers at Re dopants. These results provide useful information for developing doping strategy of MoS_2 for optoelectronic applications.

1 Introduction

Recently, two-dimensional (2D) transition metal dichalcogenides (TMDs) have drawn considerable attention as new forms of nanoscale materials $^{1-3}$. As the most extensively studied member of TMDs, MoS_2 has shown several attractive properties such as layer-dependent band structure 4,5 , valley-selective optical coupling $^{6-8}$, large exciton and trion binding energy $^{9-11}$, and strong nonlinear optical responses $^{12-14}$. Due to these novel properties, MoS_2 has been regarded as a promising candidate for applications of field-effect transistors 15 , integrated circuits 16 , solar cells 17 , photodetectors 17 , and light-emitting diodes 18 .

For device applications, it is necessary to modulate and control electronic and optical properties of the material. It has been well known that lattice imperfections, such as dopants, often determine physical and chemical properties of crystalline solids. In the development of semiconductor industry, doping is widely used to control the type and density of charge carriers and tailor the charge transport properties. For example, p-n junctions formed by spatially selective doping of silicon is the cornerstone of mod-

Electron paramagnetic resonance measurements showed that rhenium is the major type of impurity in natural occurring MoS_2 crystals, with a density in the range of 10^8-10^{12} cm⁻² per layer²⁴. Most Re atoms are substitutional dopants at Mo sites and do not migrate, as revealed by scanning transmission electron microscopy measurements²⁰. They do not alter the atomic structure of the system²⁵. Controllable Re doping in synthesized MoS_2 was also demonstrated 20,26 . Substitutional Re dopants give rise to shallow donor states that are about 89 meV below the conduction band in bulk MoS_2 ²⁴. Therefore, Re-doping is n-type, as confirmed by both transport measurements ²⁰ and computational studies 20,27 .

Despite of these efforts on understanding various basic aspects of Re dopants in MoS₂, their effects on optical properties and dynamical properties of photocarriers have not been studied. Optical properties and photocarrier dynamics are important for most optoelectronic applications. For example, photocarrier lifetime often limits the efficiency of photovoltaic devices. Here we report a comprehensive study on the effects of Re dopants on Raman scattering, optical absorption, photoluminescence, and photocarrier dynamics of both 1L, few layer, and bulk MoS₂. We found

ern electronic technology. In developing 2D materials, it has been recognized 19 that doping will play important roles to control the electrical 20 , optical 21,22 , and magnetic properties 23 .

^a National Synchrotron Radiation Laboratory, University of Science and Technology of China, Hefei, Anhui, 230029, China

b Department of Physics and Astronomy, The University of Kansas, Lawrence, Kansas 66045

that Re dopants with a concentration of 0.6% induce red-shift and broadening of the major phonon Raman modes, Red-shift and broadening of excitonic absorption resonances, more than 10 fold of photoluminescence (PL) quenching, reduction of photocarrier lifetime by about 20 times, and suppression of exciton formation. These results reveal the important impact of Re doping on optoelectronic properties of MoS₂. The information is valuable for evaluating strategies of modulating electronic and optical properties of MoS₂ for targeted applications.

Experimental section

MoS₂ crystals were acquired from 2DSemiconductors. These bulk crystals were prepared by chemical vapor transport at high vacuum of 10⁻⁶ Torr and high temperature of 1050°C. Elemental precursors of Mo, S, and Re with 6N purity were used. MoCl₅ was introduced as the transport agent to eliminate transition metal contamination. For Re-doped crystals, the dopants were introduced as a free material into the sealed vacuum quartz tube. The mixture was kept at high temperature for 3 months. The temperature difference between hot zone (precursor) and cold zone (product) was 50°C. The Re doping concentration is 0.6 % by weight, which corresponds to 0.516 mol %.

Monolayer (1L) and few-layer samples were obtained by mechanical exfoliation from these bulk crystals by adhesive tape, which were transferred to 0.5 mm quartz substrates for optical measurements. The thickness of the samples were determined by their reflection contrasts ^{28,29}. The samples were kept under the ambient condition at 300 K for all the measurements.

To obtain absorbance spectrum, reflection contrast measurements were performed. A 800-nm and 100-fs laser pulse from a modelocked Ti-doped sapphire laser was used to generate supercontinuum radiations from a photonic-crystal fiber. This broadband light was focused to the samples on quartz substrates by an objective lens to a spot size of about 2 µm. The reflected light from the sample was collected by the same objective lens and measured by a spectrometer. It has been established that for a thin TMD layer on a thick and transparent substrate, the absorbance of the TMD layer $A = (1/4) (n_q^2 - 1) (R_s - R_q) / R_q$, where n_q is the index of refraction of the quartz substrate, and R_s and R_q are the reflectance of the sample (on quartz) and the substrate ³⁰. Hence, by measuring the reflectance spectra with the laser spot located on the sample or the bare substrate, respectively, we can obtain the absorbance spectrum of the sample. Photoluminescence (PL) spectra were measured with the same spectroscopic setup, but with a 405-nm and 30- μ W continuous-wave laser. The PL was collected in reflection geometry. A set of filters was placed before the spectrometer to block unwanted light.

Time-resolved differential reflection measurements were performed with a setup based on a femtosecond laser system, which is composed of a 80-MHz passively modelocked Ti-doped sapphire laser and an optical parameteric oscillator. The 100-fs and 776-nm output of the sapphire laser was split to two parts. About 10 % of the beam is focused to a beta barium borate crystal to obtain its second harmonic at 388 nm, used as the pump pulse. The rest of the 776-nm beam is used to pump the optical parametric oscillator. Its output of 1320 nm is focused to another beta barium borate crystal to generate a 660-nm pules, used as the probe. The probe is centered on the peak of PL of the samples, i.e., on its exciton resonance. The pump photon energy is above the band gap of MoS2.

The pump and the probe beams were combined by a beamsplitter and focused to the sample by an objective lens to a spot size of about 2 μ m in full-width at half-maximum (FWHM). The reflected probe is collimated by the objective lens and was measured by a biased Si photodiode. Lock-in technique was used to measure the differential reflection, which is defined as the normalized change of the probe reflection caused by the pump, $\Delta R/R_0 = (R-R_0)/R_0$, where R and R_0 are the reflection of the probe with and without the presence of the pump beam, respectively 31 .

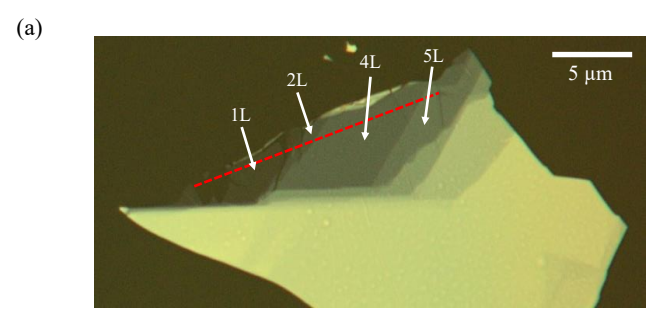
Results and discussion

3.1 Sample Characterization

Figure 1 shows the optical microscope image of a Re-doped MoS₂ flake that was fabricated by mechanical exfoliation and then transferred to a 0.5-mm quartz substrate. The flake contains regions of different thickness. We analyzed the green channel contrast across a line over multiple regions [the red dashed line in Figure 1(a)]. Here, the contrast is defined as $[C(x)-C_s]/C_s$, where C(x) and C_s are the green channel counts of a pixel at x and the average counts of the substrate, respectively. The result is shown in Figure 1(b). One can clearly see a step-like contrast variation, with a step of about 11 %. Previously, it has been shown that for thin TMD flakes on transparent substrates, the contrast is proportional to the number of layers ^{28,29}. The step of 11 % is in well agreement of the previously established values for TMDs ^{28,29}. We note that in other Re-doped MoS2 samples fabricated (but not used for optical measurements), the minimal contrast is also close to 11 %. Hence, it is safe to conclude that the contrast of 11 % corresponds to 1L. We can thus identified various regions of the sample as 1L, 2L, 4L, and 5L, as labeled in Figure 1.

3.2 Raman Spectroscopy

The samples were characterized by Raman spectroscopy with a 488-nm and 1 mW laser beam. The red symbols in Figure 2(a) show Raman spectra of Re-doped MoS2 flakes with different thicknesses, as indicated in the legend. For comparison, Raman spectra of undoped MoS2 1L and bulk were also measured under the same conditions. In all the spectra shown in Figure 2(a), the left and right peaks can be assigned to the in-plane E_{2g}^1 (around 380 cm⁻¹) and out-of-plane A_{1g} (around 400 cm⁻¹) phonon modes, respectively, according to previous studies 32,33. To obtain the precise peak position and FWHM of the two modes, each spectrum was fit by the sum of two Lorentz functions, as indicated by the curves in Figure 2(a). Figure 2(b) summarizes the peak positions of the two phonon modes. We observe an increase (decrease) of the Raman shift for the A_{1g} (E_{2g}^1) mode with sample thickness. This trend is consistent with previous reports on undoped ${
m MoS_2}\,^{32,33}$. We find that the E^1_{2g} mode of Re-doped ${
m MoS_2}$ is red-shifted by about 1.1 cm⁻¹ compared to undoped MoS₂, while the A_{1g} peak is almost unchanged. For bulk, both modes show



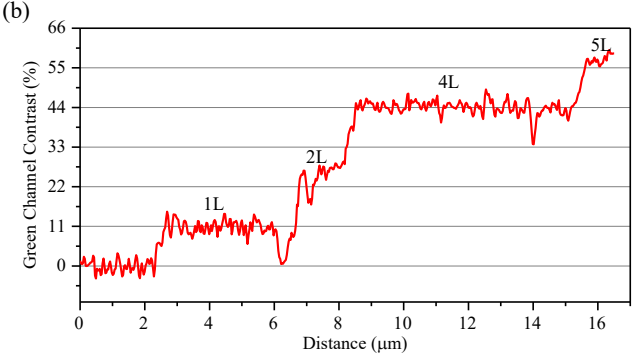


Fig. 1 (a) Optical microscope image of a Re-doped MoS_2 flake on a quartz substrate, obtained by mechanical exfoliation (b) Optical contrast of the green channel along the red dashed line in (a)

red-shifts of about 1 cm^{-1} with respect to undoped bulk MoS_2 .

Based on previous reports 34,35 , application of strain can redshift and even split the E^1_{2g} mode of MoS $_2$ 1L, while the A_{1g} mode shows no measurable shift. In our Re-doped MoS $_2$ 1L sample, the red-shift of the E^1_{2g} indicates that the substitutional Re atoms introduce strain to the lattice, as can be expected from their twice-larger atom size. The A_{1g} mode is strongly coupled to the electrons. The broadening of the A_{1g} mode can be attributed to the doping carriers introduced by Re 20 .

3.3 Steady-State Optical Properties

We next studied steady-state optical properties of these samples. Figure 3(a) and (b) show the absorbance spectra of the undoped and Re-doped MoS_2 1L samples, respectively. For the undoped sample, the A - and B-exciton resonances were clearly observed, which are consistent with previous reports 36 . In the doped sample, both excitonic resonances are red-shifted and broadened, which could be attributed to the effect of Re-related defect states 20,27 . Although theory showed that Re dopants introduce deep impurity levels in free-standing MoS_2 1L 37 , the dielectric screening of the surrounding materials, such as the substrate, reduces the Coulomb potential and results in shallow energy levels 24,37 .

Figure 3(c) shows the PL spectrum of the undoped MoS_2 1L. Both the peak position and the PL yield are consistent with previous studies on samples of same type³⁸. The PL spectra of the Re-doped MoS_2 flakes were measured under the same conditions. As shown in Figure 3(d), the PL yield of the 1L is about 15 times smaller than the undoped MoS_2 1L. The 2L sample shows a PL peak that is about 10 times weaker than the 1L. Other doped

samples (4L, 5L, and bulk) do not show detectable PL peaks. The thickness dependent PL of the Re-doped samples further confirms that the sample with smallest optical contrast of 11 % is 1L. The strong PL quenching by Re-doping can be attributed to capture of photocarriers by the defect states and other defect-related nonradiative recombination of photocarriers. Furthermore, it is interesting to note that the PL peak of the Re-doped 1L shows a small blue-shift and no broadening, both in contrast to the absorption measurements. This could be attributed to the different impacts of the dopants on light absorption and emission processes. However, further studies are necessary to fully understand this feature.

3.4 Photocarrier Dynamics

To better investigate effect of Re-dopants on photocarrier dynamics in MoS2, we first studied photocarrier dynamics in undoped MoS₂ 1L. The sample was pumped by a 388-nm pulse. Differential reflection of a 660-nm probe, tuned to the peak of the Aexciton of MoS2, was measured as a function of the probe delay, which is defined as the time delay of the probe pulse with respect to the pump. Figure 4 shows the results for three different values of the pump fluence. Based on the absorption coefficient of MoS₂ 1L at 388 nm³⁹, a pump pulse with a fluence of 1 μ J cm⁻² injects a peak carrier density of about 2×10^{11} cm⁻². We find that the decay can be fit by a single-exponential function. The decay constant is independent of the pump fluence, with an average value of 22 ± 3 ps. Since exciton formation time in TMD 1Ls are as short as 1 ps ^{40–42}, the photocarriers are in the form of excitons on 20ps time scale. The decay time is thus attributed to exciton lifetime in undoped MoS₂ 1L.

Next, we studied the photocarrier dynamics in Re-doped MoS_2 1L. The differential reflection of the 660-nm probe was measured with various values of the 388-nm pump fluence, as shown in Figure 5(a). Clearly, the signal decays on a much faster time scale. Exponential fits [curves in (a)] were used to determine the decay time constant, which was found to be independent of the pump fluence, as shown in Figure 5(b) (blue symbol and right axis). The decay time is about 1 ps, which is about 20 times shorter than the undoped sample. We attribute this ultrashort photocarrier lifetime to the efficient Auger recommbination of carriers by Redopants. The photocarrier lifetime is comparable to the exciton formation time $^{40-42}$, indicating that the Re-dopants suppress the formation of excitons. The lack of density dependence of the carrier lifetime indicates that exciton-exciton annihilation 43,44 plays a minor role here.

The red symbols (left axis) of Figure 5(b) show the peak signal as a function of the pump fluence (bottom axis) and injected carrier density (top axis). The data can be fit by a saturation model, $\Delta R/R_0 \propto N/(N+N_{sat})$, where $N \text{ cm}^{-2}$ is the injected carrier density and $N_{sat}=1.8\times10^{11}$ is the saturation density 31 . To ensure that the probe senses the carrier-induced change of the A-exciton resonance, we repeated the measurement with different probe wavelengths and with a pump fluence of 1.4 μJ cm⁻². As shown in Figure 5(c), the signal is only significant when the probe is near the exciton resonance. We note that both positive (photobleaching) and negative (photoninduced absorption) signals were ob-

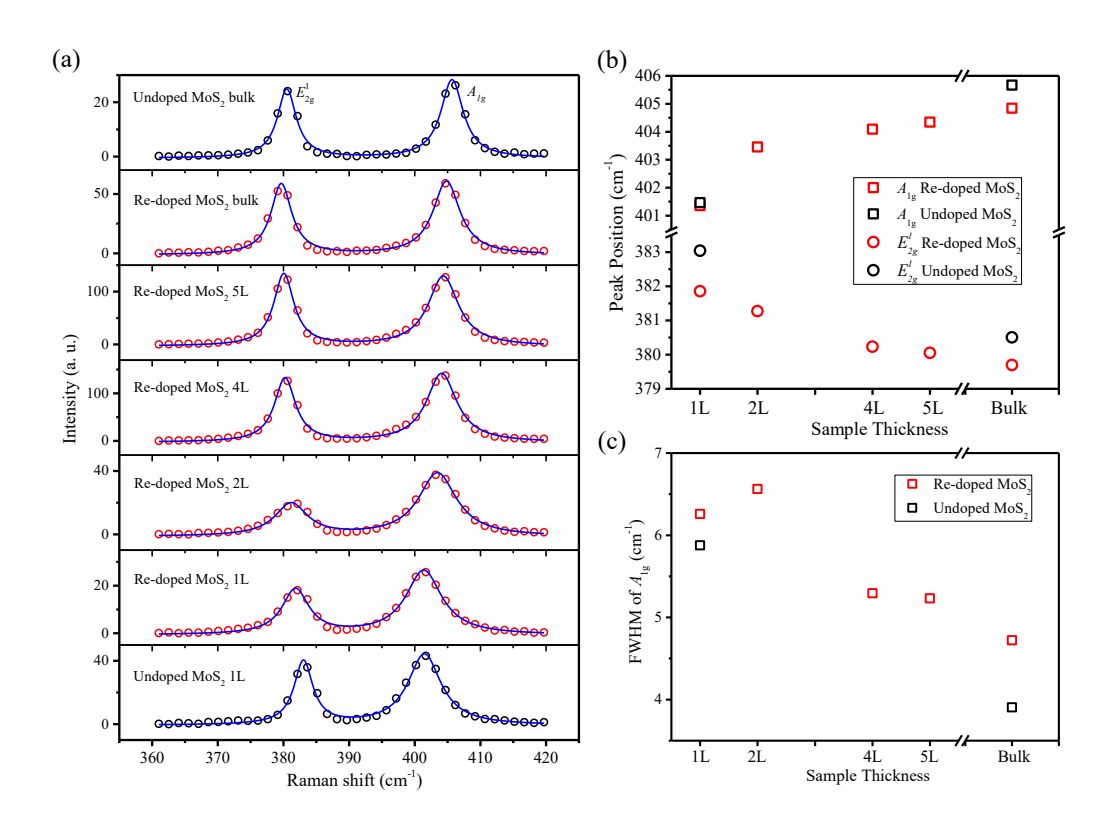


Fig. 2 (a) Raman spectra from regions of different thicknesses of the Re-doped MoS₂ flake (red) and from undoped MoS₂ 1L and bulk samples (black). The blue curves are fits with two Lorentz functions. (b) Peak position of E_{2g}^1 and A_{1g} phonon modes obtained from the fits. (c) Full width at half maxima (FWHM) of A_{1g} peak obtained from the fits.

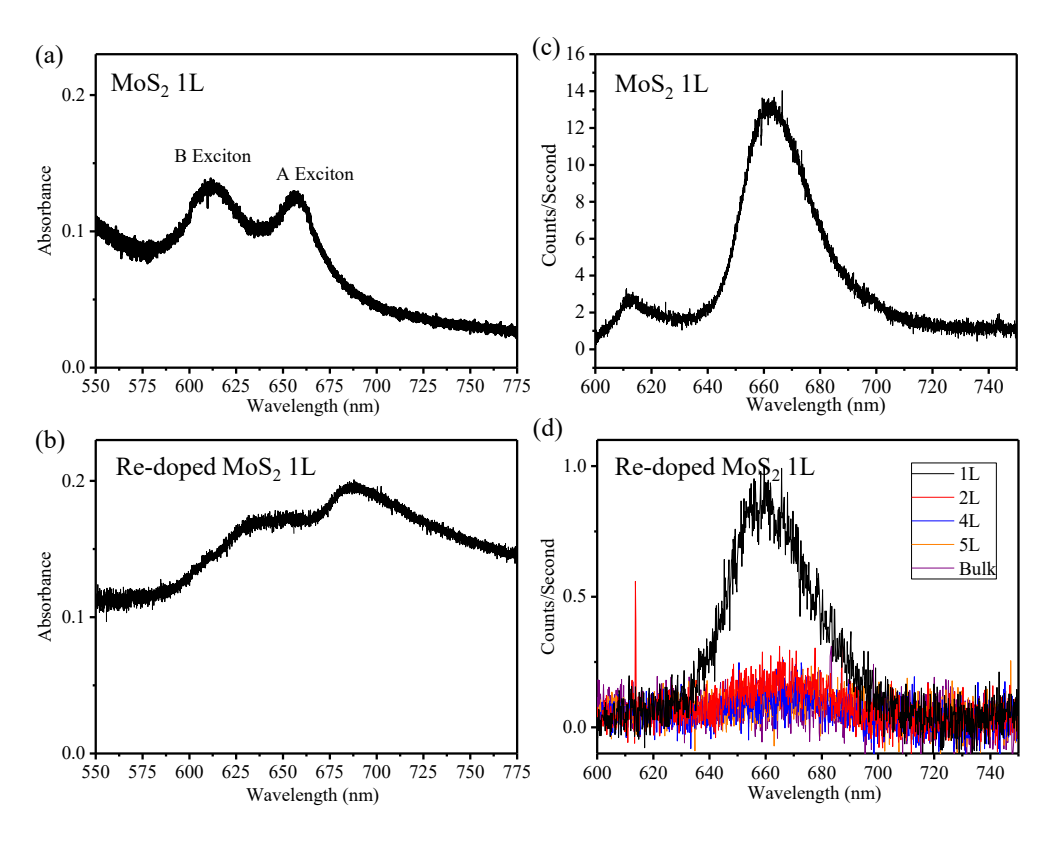


Fig. 3 (a) and (b) Absorbance spectra of the undoped (a) and Re-doped (b) MoS_2 1L (c) PL spectrum of the undoped MoS_2 1L. (d) PL spectra of the Re-doped MoS_2 flakes with different numbers of layers.

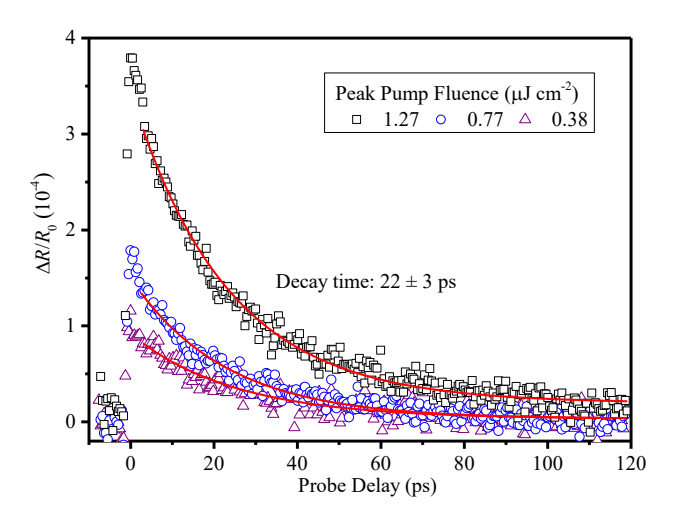


Fig. 4 Differential reflection of the undoped MoS $_2$ 1L with a pump of 388 nm and a probe of 660 nm. The pump fluences used are indicated in the legend. Red curves are exponential fits with an averaged exciton lifetime of about 22 ps.

served. This is similar to results from undoped MoS₂ ⁴⁵.

Finally, we repeated the measurement on a Re-doped MoS_2 bulk sample. The results are summarized in Figure 5(d) - (f). The decay of the signal is found to be slightly slower than the 1L sample, and is still independent of the pump fluence, as shown in (d) and (e). The peak signal is proportional to the injected carrier density (e), and depends sensitively on the probe wavelength (f). These results solidify our conclusion that Re-dopants significantly reduces the photocarrier lifetime in MoS_2 .

The 20-fold reduction of photocarrier lifetime by Re-dopants is well consistent with 16-fold PL quenching. The difference could be attributed to various processes associated with the steady-state and dynamical measurements. Furthermore, the picosecond carrier lifetime is also consistent with carrier transport properties that was previously studied. With a lattice constant (Mo-Mo) of 0.32 nm and a weight doping concentration of 0.6 %, the average distance between two dopants is on the order of 10 nm. Consider diffusive motion of photocarriers, the average distance an electron-hole pair travel in time τ is $L^2 = D\tau$, where D is the diffusion coefficient of photocarriers. Using $L \sim 10$ nm and $\tau \sim 1$ ps, we find $D \sim 1 \text{ cm}^2 \text{ s}^{-1}$. Previous measurements have shown that for TMD 1Ls, the exciton diffusion coefficient is on the order of $10 \text{ cm}^2 \text{ s}^{-146-51}$. Since the Re-dopants are expected to reduce the mobility and diffusion coefficient of the sample by introducing additional scattering mechanisms, We find the picosecond photocarrier lifetime is reasonably consistent with the diffusion-limited Auger recombination at Re sites.

The reported effects of Re doping on photocarrier dynamics and optical properties of MoS_2 are important for developing doping strategies for optoelectronic applications. It is also useful for understanding behaviors of nominally undoped MoS_2 , since Re is the most common impurity in MoS_2 . Furthermore, the effective control of photocarrier lifetime by Re doping can be utilized in developing fast optoelectronic devices. It has been known dur-

ing the development of GaAs-based optoelectronic devices that an ultrashort photocarrier lifetime can be advantageous for some applications. For example, low-temperature-grown GaAs thin films with a photocarrier lifetime of less than 1 ps can achieve high-speed terahertz emitters and detectors, because the carriers injected by the femtosecond gating pulse can quickly recombine ⁵². Low-temperature-grown Be-doped InGaAs/InAlAs multiple quantum wells with short photocarrier lifetime can achieve ultrafast optical switching ⁵³. Hence, Re-doped MoS₂ can be explored for 2D-materials-based high-speed optoelectronic devices.

4 Conclusion

In conclusion, we have performed a comprehensive study on the effect of Re dopants on optical properties and photocarrier dynamics in MoS₂ monolayer and bulk samples. We have found that with 0.6 % (weight) Re doping, MoS₂ maintains its lattice structure and band structure, as evident by the Raman, absorption, and photoluminescence spectra that are similar to undoped samples. Re atoms introduce lattice strain and charge doping, which are probed by red-shift and broadening of the phonon modes in Raman spectra. Compared to undoped samples, we observed a 15-fold PL quenching in the Re-doped MoS₂ monolayer. The photocarrier lifetime was reduced to 1 ps, which is about 20 times shorter than in the undoped monolayer. Similarly short photocarrier lifetime was also obtained in a doped bulk sample. These results are valuable to evaluating strategies of modulating electronic and optical properties of MoS₂ for targeted applications.

Acknowledgment

This material is based upon work supported by the National Science Foundation of USA (Nos. DMR-1505852, DMR-1337737, DMR-1508494), US Army Research Office grant W911NF-16-1-0029, National Natural Science Foundation of China (No. U1732148), and Technological Development Grant of Hefei Science Center of CAS (2014TDG-HSC002).

References

- 1 F. Schwierz, J. Pezoldt and R. Granzner, *Nanoscale*, 2015, 7, 8261–8283.
- 2 Z. Lin, A. McCreary, N. Briggs, S. Subramanian, K. H. Zhang, Y. F. Sun, X. F. Li, N. J. Borys, H. T. Yuan, S. K. Fullerton-Shirey, A. Chernikov, H. Zhao, S. McDonnell, A. M. Lindenberg, K. Xiao, B. J. LeRoy, M. Drndic, J. C. M. Hwang, J. Park, M. Chhowalla, R. E. Schaak, A. Javey, M. C. Hersam, J. Robinson and M. Terrones, 2D Mater., 2016, 3, 042001.
- 3 S. Lee and Z. Zhong, Nanoscale, 2014, 6, 13283-13300.
- 4 K. F. Mak, C. Lee, J. Hone, J. Shan and T. F. Heinz, *Phys. Rev. Lett.*, 2010, **105**, 136805.
- 5 A. Splendiani, L. Sun, Y. Zhang, T. Li, J. Kim, C. Y. Chim, G. Galli and F. Wang, *Nano Lett.*, 2010, 10, 1271–1275.
- 6 D. Xiao, G. B. Liu, W. Feng, X. Xu and W. Yao, *Phys. Rev. Lett.*, 2012, **108**, 196802.
- 7 H. Zeng, J. Dai, W. Yao, D. Xiao and X. Cui, *Nat. Nanotechnol.*, 2012, 7, 490–493.
- 8 K. F. Mak, K. He, J. Shan and T. F. Heinz, Nat. Nanotechnol.,

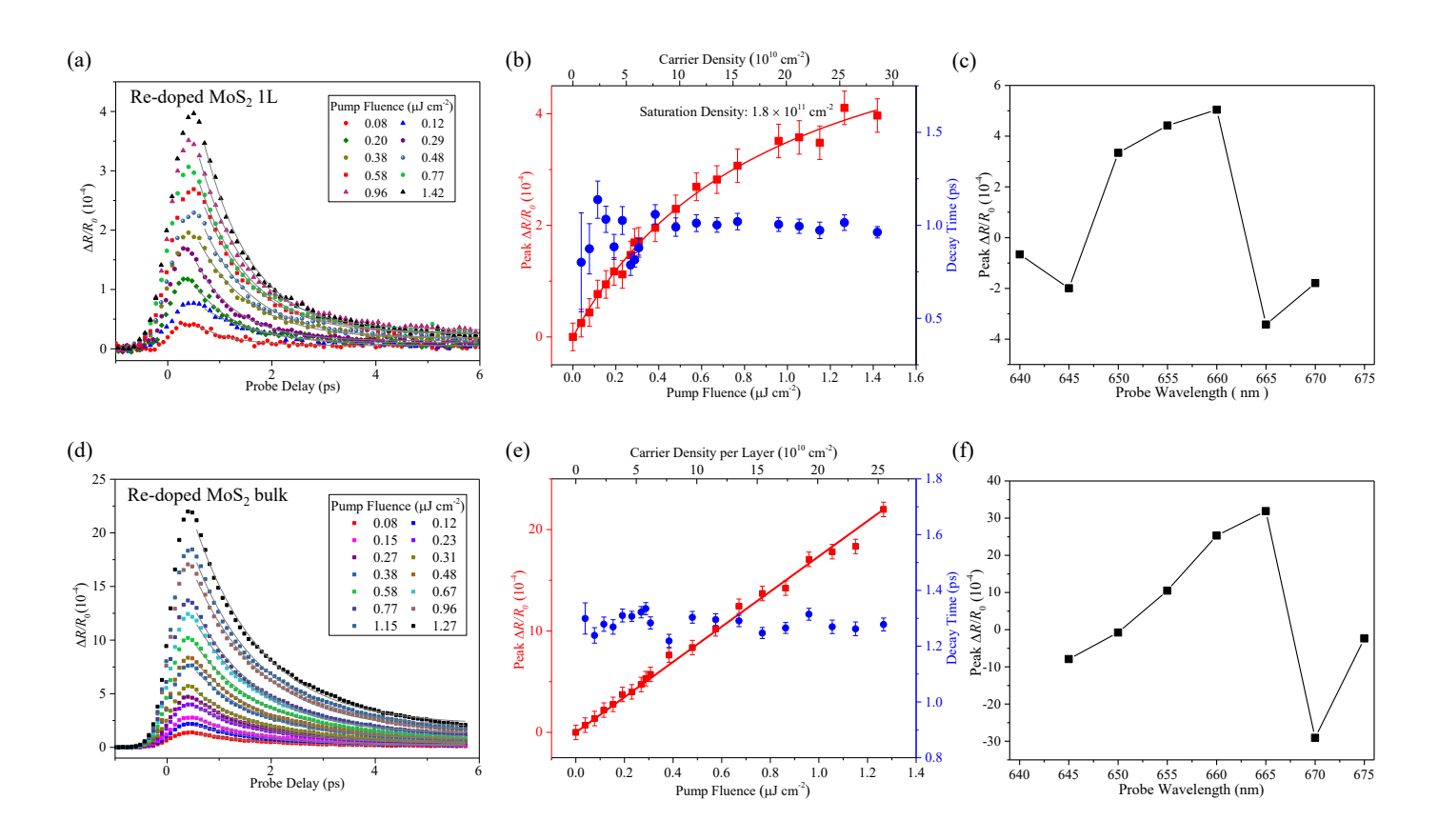


Fig. 5 (a) Differential reflection of Re-doped MoS₂ 1L measured with 388-nm pump and 660-nm probe pulses. Symbols represent data with different values of the pump fluence. Curves are exponential fits. (b) Red symbols and left axis: Peak differential reflection signal as a function of the pump fluence (bottom axis) and injected carrier density (top axis). The curve is a fit (see text). Blue symbols and right axis: Decay time constant as a function of the pump fluence and injected carrier density. (d), (e), and (f) are the same as (a), (b), and (c), respectively, for the doped bulk sample.

- 2012, 7, 494-498.
- 9 A. Chernikov, T. C. Berkelbach, H. M. Hill, A. Rigosi, Y. L. Li, O. B. Aslan, D. R. Reichman, M. S. Hybertsen and T. F. Heinz, *Phys. Rev. Lett.*, 2014, 113, 076802.
- 10 K. He, N. Kumar, L. Zhao, Z. Wang, K. F. Mak, H. Zhao and J. Shan, *Phys. Rev. Lett.*, 2014, **113**, 026803.
- 11 M. Z. Bellus, F. Ceballos, H.-Y. Chiu and H. Zhao, *ACS Nano*, 2015, **9**, 6459–6464.
- 12 N. Kumar, S. Najmaei, Q. Cui, F. Ceballos, P. M. Ajayan, J. Lou and H. Zhao, *Phys. Rev. B*, 2013, **87**, 161403.
- 13 L. M. Malard, T. V. Alencar, A. P. M. Barboza, K. F. Mak and A. M. de Paula, *Phys. Rev. B*, 2013, **87**, 201401.
- 14 Y. Li, Y. Rao, K. F. Mak, Y. You, S. Wang, C. R. Dean and T. F. Heinz, *Nano Lett.*, 2013, **13**, 3329–3333.
- 15 B. Radisavljevic, A. Radenovic, J. Brivio, V. Giacometti and A. Kis, *Nat. Nanotechnol.*, 2011, **6**, 147–150.
- 16 H. Wang, L. L. Yu, Y. H. Lee, Y. M. Shi, A. Hsu, M. L. Chin, L. J. Li, M. Dubey, J. Kong and T. Palacios, *Nano Lett.*, 2012, 12, 4674–4680.
- 17 B. W. H. Baugher, H. O. H. Churchill, Y. Yang and P. Jarillo-Herrero, *Nat. Nanotechnol.*, 2014, 9, 262–267.
- 18 Y. J. Zhang, T. Oka, R. Suzuki, J. T. Ye and Y. Iwasa, *Science*, 2014, **344**, 725–728.
- 19 Y. D. Zhao, K. Xu, F. Pan, C. J. Zhou, F. C. Zhou and Y. Chai, *Adv. Funct. Mater.*, 2017, **27**, 23.
- 20 Y. C. Lin, D. O. Dumcenco, H. P. Komsa, Y. Niimi, A. V. Krasheninnikov, Y. S. Huang and K. Suenaga, *Adv. Mat.*, 2014, 26, 2857–2861.
- 21 G. Bai, S. Yuan, Y. Zhao, Z. Yang, S. Y. Choi, Y. Chai, S. F. Yu, S. P. Lau and J. Hao, *Adv. Mater.*, 2016, **28**, 7472–7477.
- 22 G. Bai, M.-K. Tsang and J. Hao, Adv. Funct. Mater., 2016, 26, 6330–6350.
- 23 W. Jie, Z. Yang, F. Zhang, G. Bai, C. W. Leung and J. Hao, *ACS Nano*, 2017, **11**, 6950–6958.
- 24 F. D. Brandao, G. M. Ribeiro, P. H. Vaz, J. C. Gonzalez and K. Krambrock, *J. Appl. Phys.*, 2016, **119**, 235701.
- 25 B. Sachs, L. Britnell, T. O. Wehling, A. Eckmann, R. Jalil, B. D. Belle, A. I. Lichtenstein, M. I. Katsnelson and K. S. Novoselov, *Appl. Phys. Lett.*, 2013, **103**, 251607.
- 26 L. Yadgarov, R. Rosentsveig, G. Leitus, A. Albu-Yaron, A. Moshkovich, V. Perfilyev, R. Vasic, A. I. Frenkel, A. N.Enyashin, G. Seifert, L. Rapoport and R. Tenne, *Angew. Chem. Int. Ed*, 2012, 51, 1148.
- 27 H. P. Komsa and A. V. Krasheninnikov, *Phys. Rev. B*, 2015, **91**, 125304.
- 28 D. A. Chenet, O. B. Aslan, P. Y. Huang, C. Fan, A. M. van der Zande, T. F. Heinz and J. C. Hone, *Nano Lett.*, 2015, **15**, 5667–5672.
- 29 Q. Cui, R. A. Muniz, J. E. Sipe and H. Zhao, *Phys. Rev. B*, 2017, 95, 165406.
- 30 O. B. Aslan, D. A. Chenet, A. M. van der Zande, J. C. Hone

- and T. F. Heinz, ACS Photon., 2016, 3, 96-101.
- 31 F. Ceballos and H. Zhao, *Adv. Funct. Mater.*, 2017, **27**, 1604509.
- 32 C. Lee, H. Yan, L. E. Brus, T. F. Heinz, J. Hone and S. Ryu, *ACS Nano*, 2010, **4**, 2695.
- 33 H. Li, Q. Zhang, C. C. R. Yap, B. K. Tay, T. H. T. Edwin, A. Olivier and D. Baillargeat, *Adv. Funct. Mater.*, 2012, 22, 1385–1390.
- 34 B. Chakraborty, A. Bera, D. V. S. Muthu, S. Bhowmick, U. V. Waghmare and A. K. Sood, *Phys. Rev. B*, 2012, **85**, 161403.
- 35 C. R. Zhu, G. Wang, B. L. Liu, X. Marie, X. F. Qiao, X. Zhang, X. X. Wu, H. Fan, P. H. Tan, T. Amand and B. Urbaszek, *Phys. Rev. B*, 2013, 88, 121301.
- 36 K. P. Dhakal, D. L. Duong, J. Lee, H. Nam, M. Kim, M. Kan, Y. H. Lee and J. Kim, *Nanoscale*, 2014, **6**, 13028–13035.
- 37 J. Y. Noh, H. Kim, M. Park and Y. S. Kim, *Phys. Rev. B*, 2015, **92**, 115431.
- 38 F. Ceballos, P. Zereshki and H. Zhao, *Phys. Rev. Mater.*, 2017, 1, 044001.
- 39 H.-L. Liu, C.-C. Shen, S.-H. Su, C.-L. Hsu, M.-Y. Li and L.-J. Li, *Appl. Phys. Lett.*, 2014, **105**, 201905.
- 40 A. Thilagam, J. Appl. Phys., 2016, 120, 124306.
- F. Ceballos, Q. Cui, M. Z. Bellus and H. Zhao, *Nanoscale*, 2016,
 11681–11688.
- 42 P. Steinleitner, P. Merkl, P. Nagler, J. Mornhinweg, C. Schuller, T. Korn, A. Chernikov and R. Huber, *Nano Lett.*, 2017, 17, 1455–1460.
- 43 N. Kumar, Q. Cui, F. Ceballos, D. He, Y. Wang and H. Zhao, *Phys. Rev. B*, 2014, **89**, 125427.
- 44 D. Sun, Y. Rao, G. A. Reider, G. Chen, Y. You, L. Brezin, A. R. Harutyunyan and T. F. Heinz, *Nano Lett.*, 2014, **14**, 5625–5629.
- 45 X. Zhang, D. He, L. Yi, S. Zhao, J. He, Y. Wang and H. Zhao, *Nanoscale*, 2017, **9**, 14533.
- 46 R. Wang, B. A. Ruzicka, N. Kumar, M. Z. Bellus, H.-Y. Chiu and H. Zhao, *Phys. Rev. B*, 2012, **86**, 045406.
- 47 N. Kumar, Q. Cui, F. Ceballos, D. He, Y. Wang and H. Zhao, *Nanoscale*, 2014, **6**, 4915–4919.
- 48 Q. Cui, F. Ceballos, N. Kumar and H. Zhao, ACS Nano, 2014, 8, 2970–2976.
- 49 J. He, D. He, Y. Wang, Q. Cui, F. Ceballos and H. Zhao, *Nanoscale*, 2015, **7**, 9526.
- 50 Q. Cui, J. He, M. Z. Bellus, M. Mirzokarimov, T. Hofmann, H.-Y. Chiu, M. Antonik, D. He, Y. Wang and H. Zhao, *Small*, 2015, 11, 5565–5571.
- 51 F. Ceballos, M. Z. Bellus, H. Y. Chiu and H. Zhao, *Nanoscale*, 2015, **7**, 17523–17528.
- 52 M. Tani, S. Matsuura, K. Sakai and S. Nakashima, *Appl. Opt.*, 1997, **36**, 7853–7859.
- 53 R. Takahashi, Y. Kawamura, T. Kagawa and H. Iwamura, *Appl. Phys. Lett.*, 1994, **65**, 1790–1792.